Available online at www.sciencedirect.com
SCIENCE DIRECT®
Journal of Chromatography A, 1068 (2005) 249–260
JOURNAL OF CHROMATOGRAPHY A
www.elsevier.com/locate/chroma

Distribution analysis of ultra-high molecular mass poly(ethylene oxide) containing silica particles by size-exclusion chromatography with dual light-scattering and refractometric detection

Bedřich Porsch[a,*], Anette Welinder[b], Anna Körner[b], Bengt Wittgren[b]

[a] *Institute of Macromolecular Chemistry, Academy of Sciences of the Czech Republic, Heyrovsky Sq. 2, 16206 Prague 6, Czech Republic*
[b] *AstraZeneca R&D Mölndal, SE-43183 Mölndal, Sweden*

Received 15 November 2004; received in revised form 13 January 2005; accepted 27 January 2005

Abstract

Two different size-exclusion chromatography (SEC) systems, connected in-line either to a low-angle light scattering (LALS) or to a multi-angle light scattering (MALS) detector, are employed for determination of molecular mass distributions (MMD) of poly(ethylene oxide) (PEO) samples having a weight average molecular mass up to eight millions. The detrimental effect of the presence of strongly scattering silica particles in the samples on the light scattering signal can be eliminated using a suitable sample dissolution procedure utilizing silica solubility in aqueous mobile phase. The selection of flow-rate and sample concentration have a large impact on the obtained results. Hydrodynamic retardation phenomena and nonlinearity effects are shown to introduce severe errors in the molecular mass distributions unless flow-rate and sample concentration are kept at sufficiently low levels. Self-compensating ability of the dual detection in flow-rate effects is shown to be the main advantage here. A good agreement between the results obtained using LALS and MALS detection is found provided that a carefully selected angular extrapolation procedure is used in the case of MALS data. Thus, using carefully selected experimental conditions, SEC with light-scattering (LS) and refractometric detection proved to be an efficient technique for MMD characterisation also of ultra-high molecular mass (UHM) PEO polymers.

Keywords: Size-exclusion chromatography; Poly(ethylene oxide); Molecular mass distribution; Dual light scattering/refractometric detection

1. Introduction

Ultra-high molecular mass poly(ethylene oxide) (PEO) is widely used in various industrial applications as thickeners, flocculants and flow-improving agents [1]. Commercial products, which are not expected to have narrow molecular mass distributions (MMD), are usually characterized only by approximate molecular mass and solution viscosity at a fixed concentration. Although this may be adequate in large-scale uses, such as concrete pumping [1], more precise characterization of their specific pharmaceutical qualities in terms of molecular mass and its distribution is highly desirable.

Size-exclusion chromatography of ultra-high molecular mass (UHM) water-soluble polymers having broad molecular mass distributions is still a challenge. General obstacles to be expected here were summarized by Giddings [2]: (1) flow suppression in pores, (2) shear degradation, (3) non-equilibrium transport between mobile and stationary phase, (4) group of hydrodynamic phenomena termed as polarization effect, hydrodynamically induced diffusion, stress induced diffusion, and multipath effect, all of them leading to retardation of large coils, (5) hydrodynamic chromatography mode leading to accelerated elution, (6) concentration dependent partition coefficient (non-linearity).

Flow suppression in pores is necessary to maintain SEC resolution. Separation of UHM polymers requires sufficiently wide pores that must have sufficient depth to keep stag-

* Corresponding author. Tel.: +420 296 809 350; fax: +420 296 809 410.
E-mail address: porsch@imc.cas.cz (B. Porsch).

0021-9673/$ – see front matter © 2005 Elsevier B.V. All rights reserved.
doi:10.1016/j.chroma.2005.01.074

nant mobile phase. It is easy to calculate that PEO sample having $M_w = 10^6$ and $M_w/M_n = 3$ and, if described by Pearson's distribution, would contain molecules in the M range from 10^5 to 2×10^7. For the same polymer, described by Schulz–Zimm distribution, would follow the M range from 10^3 to 10^7. From PEO data of Devanand and Selzer [3], gyration radius $r_g = 388$ nm can be calculated for $M = 2 \times 10^7$ and transformed to hydrodynamic diameter ca. 600 nm using [4] $r_g/r_h = 1.33$, where r_h is hydrodynamic radius. Giddings's calculations [2] then predict a minimum column packing particle size above 15 μm to satisfy the condition of pore flow suppression for a broad PEO having not exceptionally high $M_w = 10^6$. This should be borne in mind any time when broad UHM polymers are analyzed by a SEC technique.

UHM polymers have to be expected to be particularly susceptible to shear degradation during SEC analysis. There is a common agreement that shear force, being a product of velocity gradient and solvent viscosity, is a decisive parameter here. Thus, water-soluble polymers should be more prone to shear degradation, when compared with organic polymers of the same M in tetrahydrofuran (THF), by a factor of two resulting from solvent viscosity difference. A natural requirement for lowering flow-rate to reduce velocity gradient contradicts high-speed SEC experiments here. Shear forces generated in the packed bed are assumed to be the main source of shear degradation. Barth [5] pointed out that extra-column sources of degradation (injection valve, capillary tubing and column frits) cannot be neglected because quite high shear forces can be generated especially in modern hardware optimized to minimize extra-column band broadening. Numerous studies of polymer degradation during SEC analysis have been published, mostly using narrow MMD polystyrenes in THF [6–11]. Sometimes contradictory results may be probably ascribed to the differences in extra-column hardware used by various authors. The recommended conditions [11] to avoid degradation of polystyrene ($M = 17 \times 10^6$) in THF were flow-rate ≤0.2 ml/min, column particle size 20 μm and injected concentration ≤0.01%. There is rather general agreement that below a certain critical molecular mass no chain rupture takes place at a given shear stress. This implies further difficulties in the case of polymers having broad MMD [2,12]; also, great differences in sensitivity to shear stress may be observed for different polymers, as shown by easily degradable PEO and non degradable carboxymethyl cellulose under identical conditions [13].

Non-equilibrium in the stationary phase, which is controlled by the diffusion into and out of the pores, becomes increasingly important for UHM polymers. The relevant effective diffusion coefficient is proportional to the bulk solute-solvent diffusion coefficient multiplied by an obstructive factor characterizing pore network of support particles [2]. Because bulk diffusion coefficient depends on $M^{-\alpha}$, where α is usually between 0.5 and 0.6, this effect must be also expected to vary along the MMD distribution in the case of broad UHM polymer.

Briefly speaking, retardation of UHM polymers summarized as a group of hydrodynamic phenomena [2] results from a complex flow pattern due to hydrodynamic, diffusion and inertial forces acting on very large coils in SEC columns. Several authors noticed these effects [2,5,7,9,14]; the dominant mechanism is difficult to distinguish because all of them yield particle retardation.

The hydrodynamic chromatography mode has been shown to give similar elution order to that of SEC (the largest coils eluted first) on nonporous packed beds [15,16]. This may be relevant in the case of UHM polymers as a transition region close to and above the exclusion limit of SEC columns [17,18].

Non-linearity, which manifests itself as a concentration-dependent elution volume, is related to changes of polymer hydrodynamic volume as a decisive separation parameter. Because polymer concentration varies within a polymer peak as well as along the SEC column due to successive band broadening, this effect, if present, would affect the shape of the eluted peak in a complex way. The general assumption in SEC that concentration (variable from the baseline to the peak top) is low enough to allow the use of infinite dilution approximation may not be true in the case of UHM polymers. Model calculations of concentration-dependent elution volumes [19,20] indicate a clear connection to the changes of polymer coil dimensions with concentration as manifested by concentration dependence of reduced viscosity (Huggins equation) or reduction of intensity of scattered light (second virial coefficient term). The coil overlap concentration $c^* \approx 1/[\eta]$, where $[\eta]$ is intrinsic viscosity, means a concentration where coils just touch each other in bulk solvent volume; it is mostly used as a criterion of sufficient dilution. Model Brownian dynamics simulations have shown [21] that a significant chain overlap is observed even at concentrations as low as $0.3c^*$. Hence, the concentration where coil interactions become negligible should be considerably lowered below c^*. For instance, to obtain concentration-independent elution volumes for hyaluronic acid [22], injected polymer concentration had to be reduced below 0.01% for M around 10^6. The value of $0.3c^*$ for PEO having $M = 10^7$ can be estimated to be around 0.008% using the Mark–Houwink equation for PEO from [1]. Because on-column dilution may be expected to reduce solute concentration by a factor of ten for a broad polymer sample, a very high sensitivity and baseline stability of a differential refractometer (DRI) are required.

To find conditions of a correct SEC analysis of UHM PEO, free of all effects discussed above, seems impossible if the system used is equipped with a DRI unit only, because no narrow standards exist in this range. The addition of a molecular mass-sensitive detector will allow differentiating between possible shear degradation and other flow-rate and molecular mass-dependent detrimental effects. These effects should lead to distortions of the $\log M$ versus elution volume calibration, accessible when a combination of a light-scattering (LS) and DRI detection is used. The use of a SEC column

set or a mixed bed column optimized to provide linear log M versus elution volume calibration in a sufficiently wide interval of M (in the case of SEC experiment free of the above obstacles) should then facilitate the optimization of SEC conditions.

The angular dependence of scattered intensity becomes increasingly important in the case of UHM polymers having particle sizes in the range of several hundreds of nanometers (see above). Two possibilities exist here to obtain the desirable values of scattered intensity corresponding to zero angle. The first is to use LALS detection at an angle low enough to be able to neglect the effect of angular dependence. The second one is to use a MALS detector measuring scattered intensity at many fixed angular positions and to extrapolate the obtained values to zero angle. Because the extrapolation of LS intensity to zero angle may be affected by various errors [23], the use of both LALS and MALS detectors for the same samples may provide additional information concerning reliability of angular extrapolation of LS intensity in the case of UHM polymers.

An additional difficulty, related to the extreme sensitivity of LS detection to solid dense particles/impurities, must be taken into the account in the case of UHM PEO polymers, known to contain around 3% of fumed silica particles [24]. Such particles, having broad particle size distribution and an average size 200–300 nm are strong scatterers and must be somehow removed before light-scattering experiment. However, the low-angle light-scattering (LALS) detector can see spikes from individual particles smaller than 100 nm [25]: preparative ultracentrifugation cannot be expected to remove all of them. Fortunately, amorphous silica is known to be sparingly soluble in water [26], essentially in the form of monosilicic acid, at the level 70–150 ppm at 25 °C, depending on sample history and its porosity. Kinetics of dissolution may be very slow unless the sample has a rather high specific surface [26]; this requirement should be satisfied in the case of fumed silica [27] component of PEO samples. Because the injected concentrations of UHM PEO have to be below 0.01% to prevent the obstacles mentioned above, the silica concentration would be about 3 ppm, i.e., much below its equilibrium solubility. Hence, a promising way to circumvent LS detection problems is outlined here.

It will be shown in this work that silica solubility allows trouble-free UHM PEO analysis using LS detection provided that a proper sample dissolution procedure is used.

Then, the appearance of the above mentioned obstacles will be shown to be dependent on flow-rate, sample M and its concentration and the SEC–LALS–RI experimental procedure will be optimized to obtain a correct SEC separation mechanism giving non biased molecular mass distributions. The results of comparable SEC experiments using multi-angle light-scattering detector (MALS–RI) with optimized angular extrapolations of light scattering data will be shown to agree with LALS–RI measurements under optimum SEC conditions.

2. Experimental

2.1. Materials

POLYOX® PEO samples WSR-205, WSRN-12k, WSRN-60k, WSR-301and WRS-308 having nominal molecular masses 600 000, 1 000 000, 2 000 000, 4 000 000 and 8 000 000, respectively, were products of Union Carbide Corp. (Danbury, CT, USA). According to the manufacturer, they contain butylated hydroxytoluene (< 0.1%), calcium as mixed salts (< 1%) and fumed silica (< 3%). Analytical reagent grade NaCl was obtained from Merck (Darmstadt, Germany) and used without further purification. Water was from a Millipore Milli-$Q_{PLUS}{}^{UF}$ ultrapure water purification unit (Millipore Corp., Bedford, MA, USA).

2.2. Chromatography

2.2.1. SEC–LALS/RI system (Prague)

Modular chromatograph consisted of a Pharmacia P-500 pump (Pharmacia & Upjohn, Uppsala, Sweden), a Pharmacia injection valve V-7 with 200 μl loop (Pharmacia & Upjohn, Uppsala, Sweden), a Chromatix KMX-6 LALS detector (LDC/Milton Roy, Sunnyvale, CA) and a Waters 2410 differential refractometer (Waters Assoc., Milford, MA) connected through a Black Star (Huntingdon, UK) 2308 A/D converter to an IBM-compatible computer. On-line RI–LALS arrangement allows the simultaneous determination of M and c at any elution volume ("slice"). The following relation is valid for Rayleigh scattering from polydisperse polymer/solvent system at low angle (6–7°):

$$\frac{K^* c}{R_\Theta} = \frac{1}{M_w} + 2A_2 c \quad (1)$$

where c is the concentration of scattering species, R_Θ the excess Rayleigh scattering factor, M_w the weight average molecular mass of scattering species and A_2 the second virial coefficient. $K^* = (2\pi n^2/N_A\lambda^4)\nu^2$ where n is the refractive index of the solvent, λ the wavelength in vacuo (633 nm), N_A the Avogadro constant and ν the refractive index increment of the scattering species in the solvent used. If correct separation takes place, the polymer seen at a slice is assumed to be monodisperse. Angular dependence of the scattered light is omitted at the low angle used. Polydispersity and column band broadening dilutes the sample considerably; hence, the term A_2c may be neglected if the concentration of the injected solution is low enough. Conventional calibration log M versus elution volume (V_e) is thus directly obtained. Homemade software (M. Netopilík, Institute of Macromolecular Chemistry) allows on-line data accumulation and all calculations of molecular mass distributions and their averages. A TSKgel GMPW linear (7.5 mm × 600 mm) column, particle size 17 μm, in series with (7.5 mm × 75 mm) TSKgel Guard column (both Watrex, Prague, CR) were used. No post-column filter was between the column and LALS as well as MALS detector.

2.2.2. SEC–MALS/RI system (Mölndal)

The separation column was a TSK-GEL GMPW$_{XL}$ 7.8 mm × 300 mm, particle size 13 μm, a linear mixed bed size exclusion column. The pump was a Shimadzu LC10AD liquid chromatography pump (Shimadzu Corp., Tokyo, Japan). The degasser used was a Gastorr 154 (Gastorr, Japan). The polymer samples were injected with a Perkin-Elmer 200 LC autosampler (Perkin-Elmer Corp., Norwalk, CT, USA) equipped with a 100 μl sample loop. The mobile phase was 0.10 M sodium chloride (p.a., Merck, Darmstadt, Germany) solution filtered with a 0.22 μm mixed cellulose ester filter GSWP (Millipore Corp., Bedford, MA, USA). The temperature in the carrier was approximately 297 K. A stainless steel high-pressure filter holder, 25 mm, (Millipore Corp., Bedford, MA, USA), with a 25 mm × 0.025 μm VSWP filter (Millipore Corp., Bedford, MA, USA) was connected directly to the pump on-line.

The light scattering photometer was a DAWN–EOS multi-angle light scattering instrument (Wyatt Technology, Santa Barbara, CA). Simultaneous concentration detection was performed using an Optilab DSP interferometric refractometer (Wyatt Technology, Santa Barbara, CA). Both detectors used a wavelength of 690 nm. Filtered toluene (Merck, Darmstadt, Germany) was used for calibration of the MALS detector and sodium chloride (Suprapur, Merck, Darmstadt, Germany) for calibration of the refractive index detector. The detectors at different angles in the MALS instrument were normalized to the 90° detector using low polydisperse pullulan P-50 (Shodex STANDARD P-82, Showa Denko, Tokyo, Japan). Bovine serum albumin (Sigma Chemical Co., St. Louis, MO.) was used to determine the interconnection volume between the detectors (0.129 ml). The signals from the two detectors were analyzed by ASTRA software (ASTRA for Windows 4.73) (Wyatt Technology, Santa Barbara, CA, USA). Berry plot ($[(K^*c)/R_\Theta]^{1/2}$ against $\sin^2(\theta/2)$) and random-coil-forced fit available in the software were used to extrapolate angular dependence of the $(K^*c)/R_\Theta$ term (Eq. (1)) to zero angle according to recommendations following from recently published model calculations [23]. The recovery was obtained from the ratio of the mass eluted from the column (determined by integration of the refractometer signal) to the mass injected.

The value of PEO refractive index increment dn/dc = 0.135 [3] was used in both cases.

3. Results and discussion

The evidence that a proper silica dissolution procedure can be utilised to remove detrimental spiking of LS signal follows from Fig. 1.

The LS signal from two consecutive injections of PEO 4 000 000 sample dissolved for 48 h to 0.2% solution, diluted 1:19 and stirred for 20 min to give c_{inj} 0.01%, is presented in Fig. 1a. No spikes are observed before PEO peak after the first injection and a lot of them appeared when PEO elution starts. The elution of silica particles continued far after the SEC elution interval as illustrated by the second injection of the same sample. Then, the column had to be rinsed at least with five column volumes to restore the LS baseline

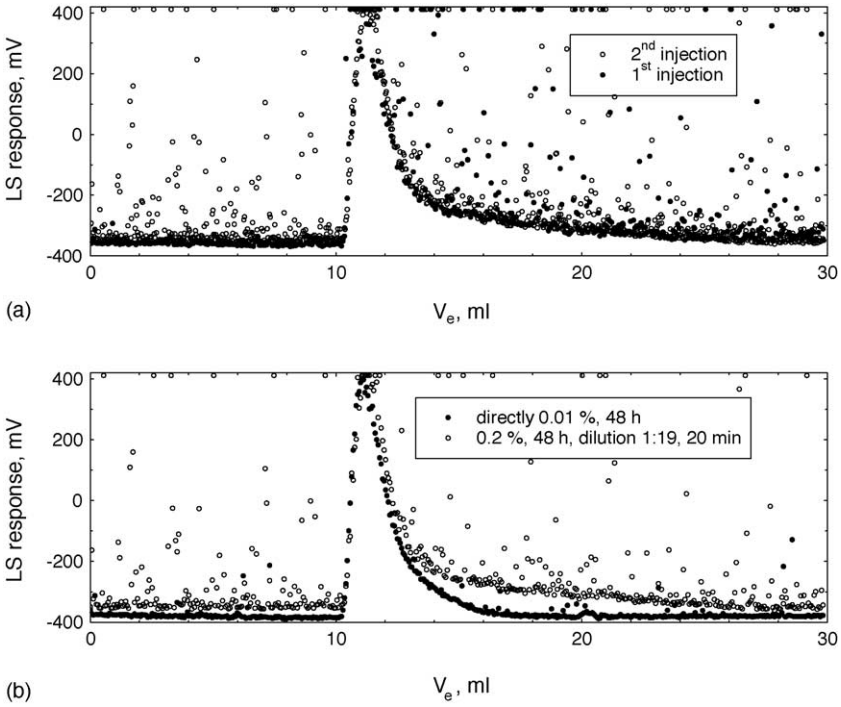

Fig. 1. LS response of PEO 4 000 000 dissolved for 48 h to 0.2% solution and injected 20 min after dilution 1:19 (a) and dissolved for 48 h to 0.01% solution (b) without any post-column filter at 0.32 ml/min.

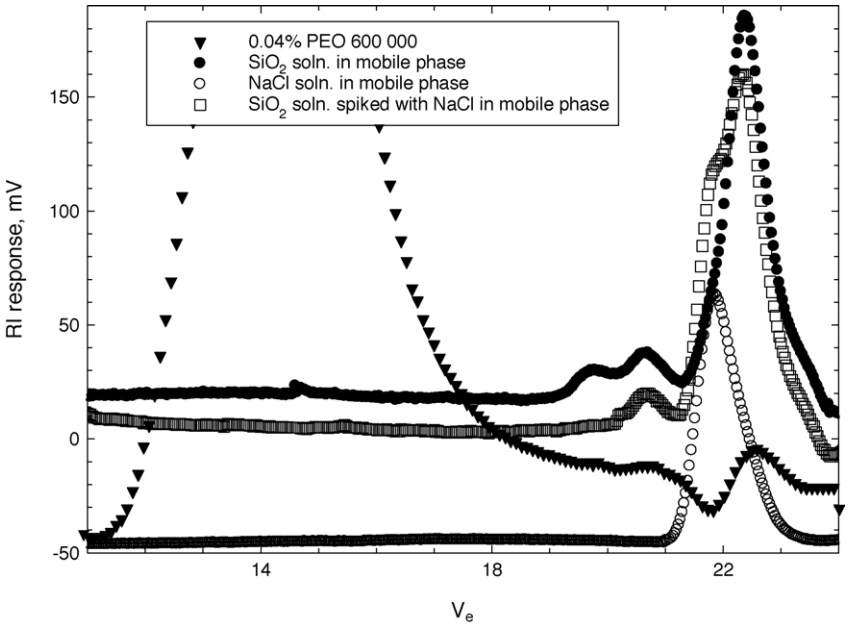

Fig. 2. Evidence of the presence of monometric silica in 0.04% solution of PEO 600 000.

free of spikes. The LS response of another sample solution prepared by direct 48-h dissolution to 0.01%, completely free of spikes, is compared with the previous solution in Fig. 1b. Because molecular masses of this sample (calculated from repeated experiments) remained constant for next 5 days, it was concluded that 48 h is a sufficient time to obtain complete silica dissolution. A qualitative evidence of the presence of monomeric silica in the sample solution follows from Fig. 2. Monosilicic acid is seen in the PEO solution as a small positive peak following small negative NaCl peak here. Hence, the 48-h dissolution of PEO samples to 0.01% (or lower) solution was used as a standard procedure in this work.

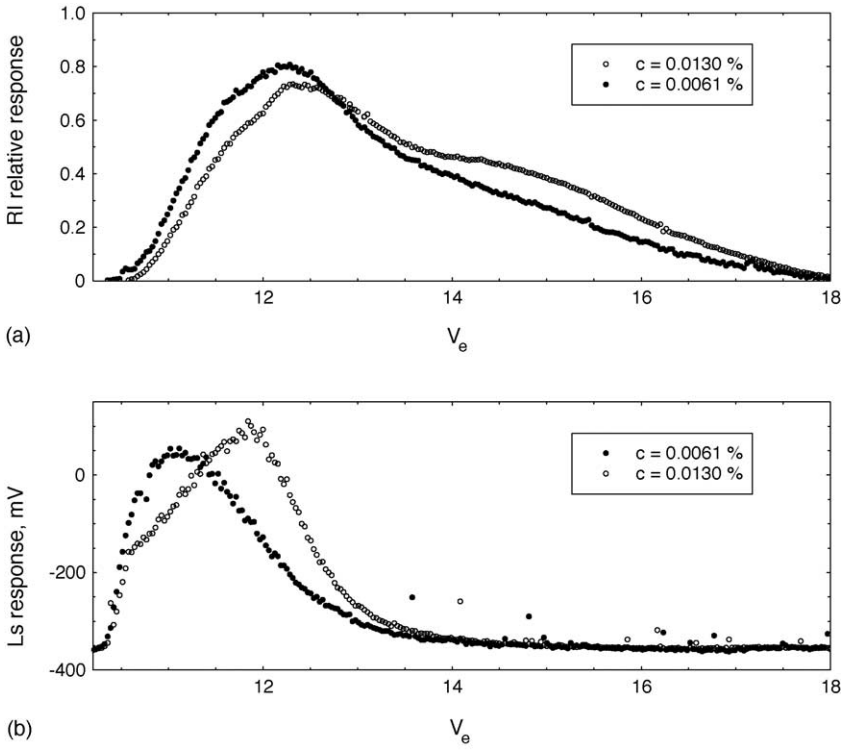

Fig. 3. RI (a) and LS (b) signal of PEO 4 000 000 as a function of injected polymer concentration at 6 ml/h.

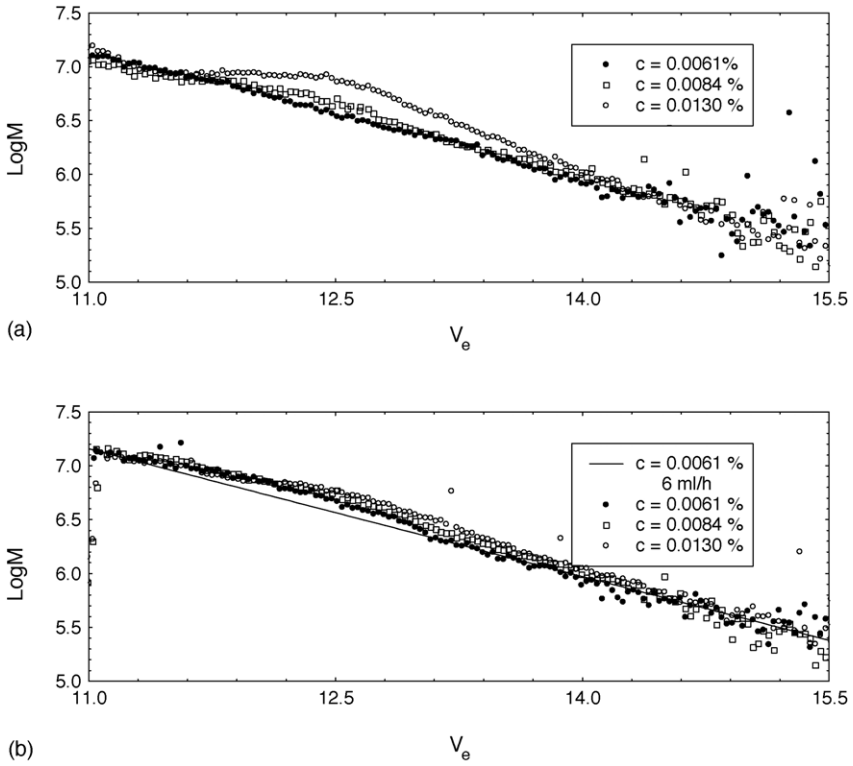

Fig. 4. $\log M = f(V_e)$ calibrations of PEO 4 000 000 as a function of injected polymer concentration at flow-rate 6 ml/h (a) and 12 ml/h (b).

The effect of variation of injected concentration of PEO 4 000 000 as seen with RI detector at flow-rate 6 ml/h is depicted in Fig. 3a. The corresponding LS traces are presented in Fig. 3b.

A clear shift of both signals indicating nonlinear SEC conditions at higher concentrations is seen. The corresponding straight line plot of $\log M = f(V_e)$ (expected for the linear column used) is obtained only at the lowest injected concentration (0.0061%) and distortion of these calibrations increases with increasing injected concentration as shown in Fig. 4a. The respective calibrations obtained at 12 ml/h are shown in Fig. 4b.

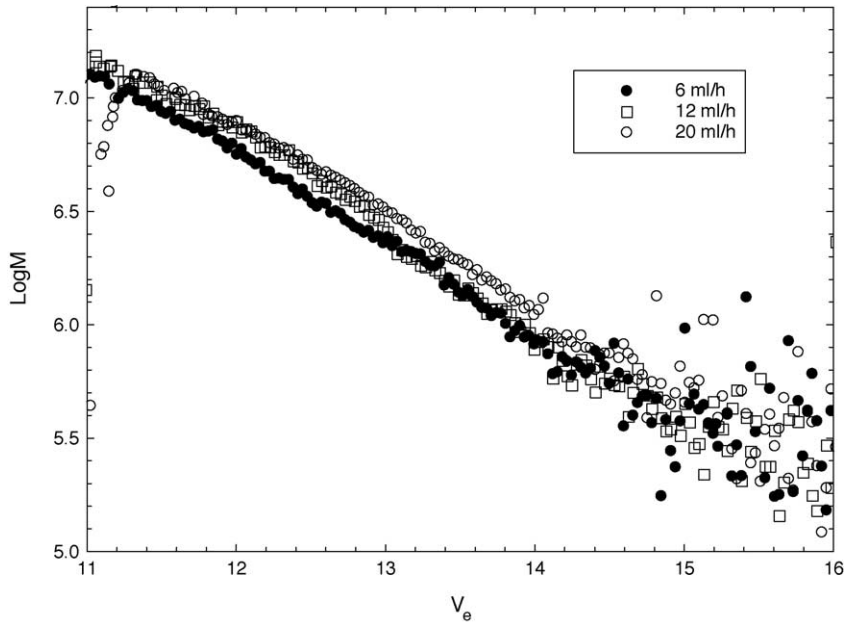

Fig. 5. $\log M = f(V_e)$ calibrations of PEO 4 000 000 as a function of flow-rate at injected polymer concentration 0.0061%.

Table 1
Molecular masses and polydispersities of PEO 4 000 000 as a function of flow-rate and concentration (SEC–LALS–RI)

Flow-rate (ml/h)	Concentration (%); (A_2 effect, %)					
	0.0061 (3.8)		0.0084 (5.1)		0.013 (8.3)	
	$M_w \times 10^{-6}$	M_w/M_n	$M_w \times 10^{-6}$	M_w/M_n	$M_w \times 10^{-6}$	M_w/M_n
6	3.95	4.9	3.91	5.0	4.08	13
12	4.02	5.7	4.02	5.7	3.97	7.5
20	4.16	4.2	–	–	5.62	1.8

A detectable deviation from linear plot obtained at 6 ml/h is visible here even at the lowest concentration and may be interpreted as the manifestation of non-equilibrium in the stationary phase and/or hydrodynamic retardation conditions. The effect of increased injection concentration at this flow-rate is somewhat smeared out indicating that concentration, non-equilibrium and hydrodynamic retardation effects are coupled to some degree. Because Fig. 4a indicates reduction of the concentration effect below the detection level at $c_{inj} = 0.0061\%$, the flow-rate was varied at this concentration (Fig. 5). Let us note that salt peaks on RI trace were always used as flow-rate markers in experiments at different flow-rates. Neither V_e changes nor salt peak broadening were observed.

Non-equilibrium and hydrodynamic retardation increasing with flow-rate is seen here as an almost parallel shift of calibrations toward higher elution volumes without any pronounced curvature. Table 1 summarises SEC results obtained for PEO 4 000 000 as a function of flow-rate and injection concentration in terms of M_w and polydispersities M_w/M_n.

As expected, the weight average molecular masses (they should be always correct being proportional to the ratio of integrated LS and RI signals) are constant within the expected experimental error unless extremely wrong experimental conditions (20 ml/h, $c_{inj} = 0.013\%$) are used. The error introduced at higher flow-rates and/or injected concentrations affects polydispersity through biased M_n value. Clearly incorrect M_w/M_n values are obtained only at $c_{inj} = 0.013\%$. The rest of results may be said to be close to the experimental error. This is corroborated by a comparison of molecular mass distributions obtained at 6 and 12 ml/h in Fig. 6.

These distributions reasonably match each other despite of 16% difference in polydispersity. This is a natural consequence of the definition of number–average determining its extreme sensitivity to the presence of low-molecular mass components. The example in Fig. 6 shows that a comparison of broad polymers only in terms of M_w/M_n may be misleading and a comparison of their molecular mass distributions should be always preferred. The results in Figs. 3–6 and in Table 1 clearly indicate that the main advantage of dual detection arrangement when compared with single RI detection setup consists in its significant self-compensation ability of flow-rate effects. Having a single SEC–RI system, there might be a temptation to interpret the RI traces in Fig. 3a as a result of shear-induced degradation. This is, of course, incorrect as follows from Table 1.

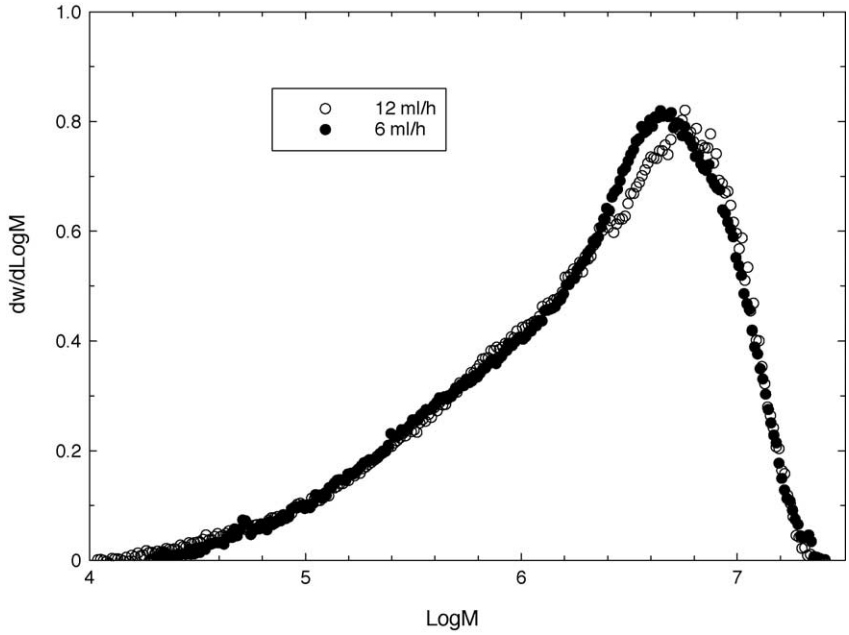

Fig. 6. Molecular mass distributions of PEO 4 000 000 obtained at 6 and 12 ml/h (injected polymer concentration 0.0061%).

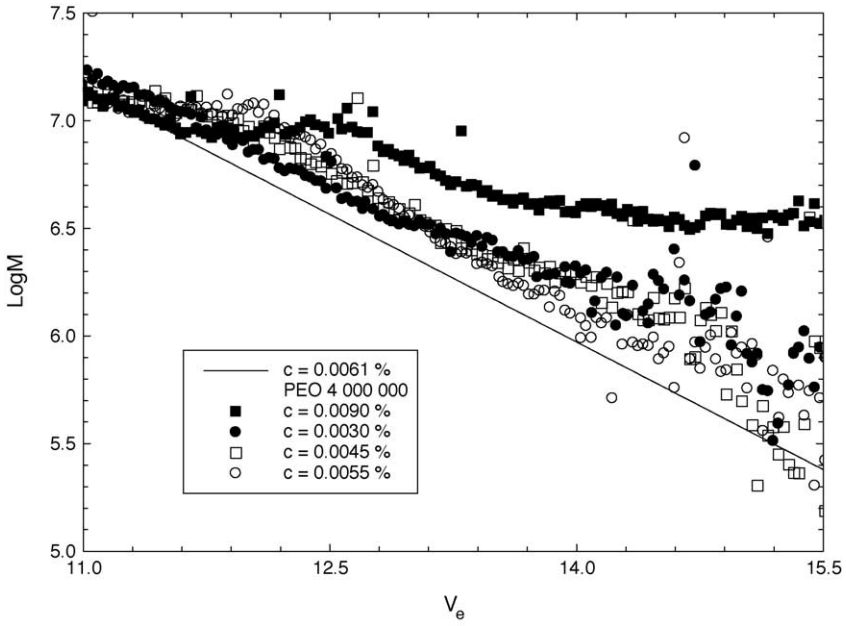

Fig. 7. $\log M = f(V_e)$ calibrations of PEO 8 000 000 as a function of injected polymer concentration at flow-rate 6 ml/h.

LALS or MALS/RI data are usually evaluated assuming zero second virial coefficient, i.e., infinite dilution conditions. Because second virial coefficient of PEO in water is known [3], its values were introduced into the software used and the data in Table 1 were recalculated. The obtained changes of M_w, expressed in % of difference from M_w calculated assuming zero second virial coefficient in Table 1, show that this error is reduced well below 5% only at concentration $c_{inj} = 0.0061\%$ but may be evaluated as not exceptionally high. It should be borne in mind that this data evaluation procedure uses the slice concentrations (variable along the concentration peak) obtained after the column passage, i.e.,

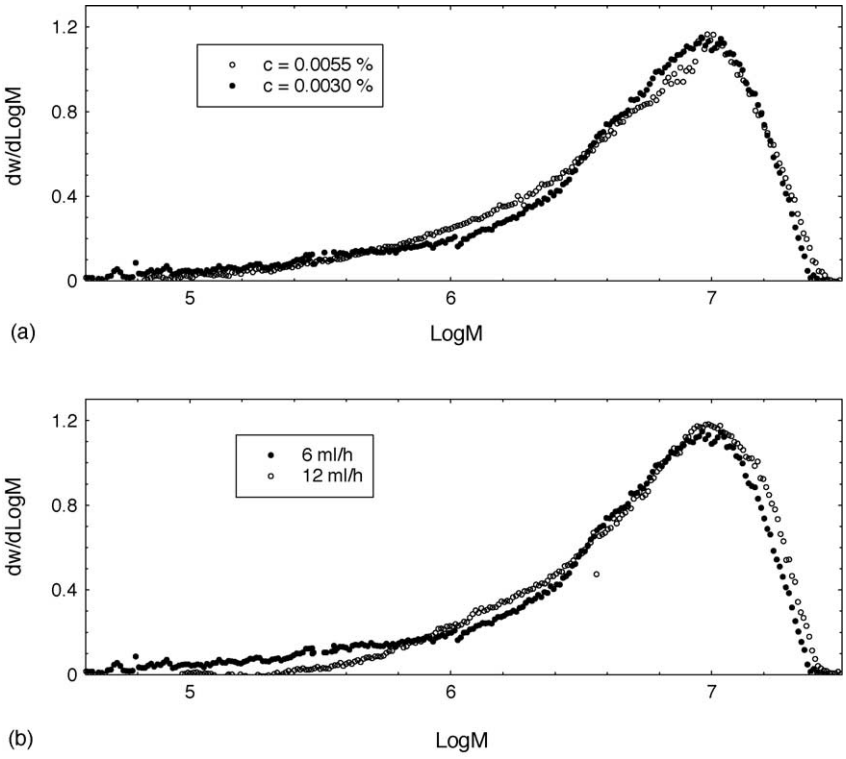

Fig. 8. Molecular mass distributions of PEO 8 000 000 as a function of injected polymer concentration at 6 ml/h (a) and of flow-rate at fixed injected polymer concentration 0.003% (b).

Table 2
Molecular masses and polydispersities of PEO 8 000 000 as a function of flow-rate and concentration (SEC–LALS–RI)

Flow-rate (ml/h)	Concentration (%); (A_2 effect, %)							
	0.0030 (3.5)		0.0045 (5.6)		0.0055 (6.5)		0.009 (8.5)	
	$M_w \times 10^{-6}$	M_w/M_n	$M_w \times 10^{-6}$	M_w/M_n	$M_w \times 10^{-6}$	M_w/M_n	$M_w \times 10^{-6}$	M_w/M_n
6	6.95	4.2	7.48	3.4	6.94	3.0	7.49	1.3
12	7.10	2.3	–	–	7.06	2.5	–	–

it includes on-column dilution. Because this dilution factor is ca. 10, the A_2 effect may be roughly 10 times larger when the separation according to size starts on the column top. Hence, it can be concluded that the distorted calibrations at higher concentrations (Fig. 4) originate mainly from the initial phase of separation (close to the column inlet) where changes of coil size with injected polymer concentration should be relevant.

As expected, the effect of injection concentration is more pronounced in the case of PEO 8 000 000 (Fig. 7).

The distortions of calibration plots $\log M = f(V_e)$ disappear only when c_{inj} is reduced to 0.003%. Moreover, an approximately parallel shift against the calibration obtained for 4 000 000 sample (Fig. 7) indicates that the flow-rate effect is not negligible in this case (cf. Fig. 5). At least a twofold reduction of flow-rate would be necessary to obtain a common linear calibration for both samples. Such experiments (duration 10 h) were performed but the difficulties with LS noise and especially RI baseline stability became too large to obtain non-biased $\log M = f(V_e)$ plots. Fortunately, a comparison of molecular mass distributions, obtained at two lowest injection concentrations (Fig. 8a) at 6 ml/h, and at $c_{inj} = 0.003\%$ and flow-rates 6 and 12 ml/h (Fig. 8b), indicates that the error in MMD obtained at $c_{inj} = 0.003\%$ and 6 ml/h should be rather small. The calculated values of M_w and M_w/M_n in Table 2 support this conclusion. Molecular masses are constant within the experimental error and a gradual reduction of polydispersity up to $c_{inj} = 0.0055\%$ and 12 ml/h is seen. Nevertheless, a too high injection concentration, 0.009%, leads to incorrect $\log M = f(V_e)$ calibration (Fig. 7) and to completely erroneous results in Table 2.

Fig. 9 shows that the concentration disturbance of $\log M = f(V_e)$ calibration appears in the case of PEO 600 000 as well. As anticipated, the only difference is that higher injection concentration is allowed in this case. Thus, the general requirements for reliable SEC analysis of these PEO samples result as follows: $c_{inj} \sim 0.1c^*$ or less and a maximum flow-rate 6 ml/h (even less if possible). The use of linear mixed bed column is highly recommended.

A comparison of $\log M = f(V_e)$ calibrations obtained for all PEO samples investigated at flow-rate 6 ml/min is presented in Fig. 10. It is seen that calibrations completely coincide up to the 2 000 000 sample. Such a common calibration should be obtained for all SEC experiments free of disturbing effects. Non-equilibrium in the stationary phase and/or hydrodynamic retardation become visible for the next sample, being more pronounced for the last one at flow-rate 6 ml/h.

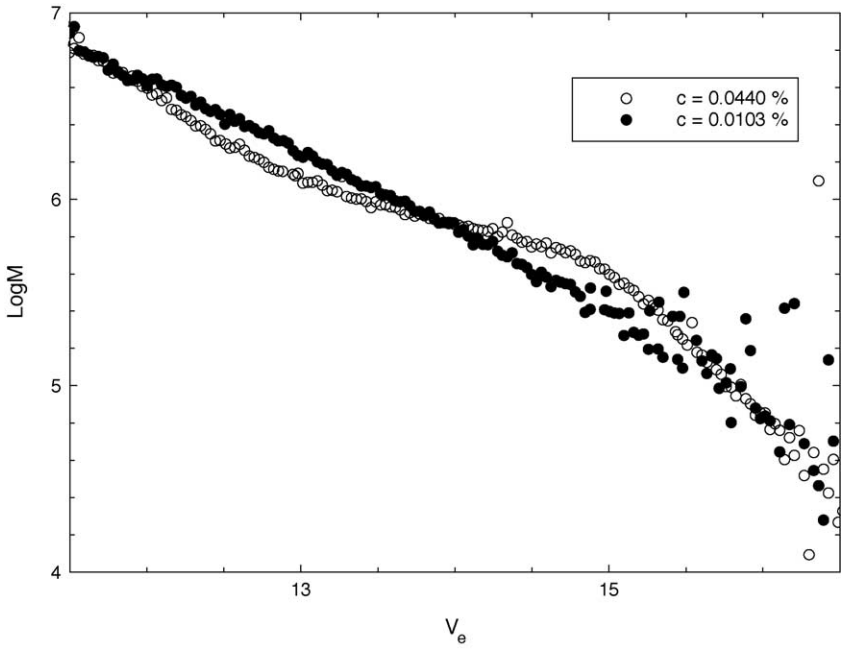

Fig. 9. $\log M = f(V_e)$ calibrations of PEO 600 000 as a function of injected polymer concentration at flow-rate 6 ml/h.

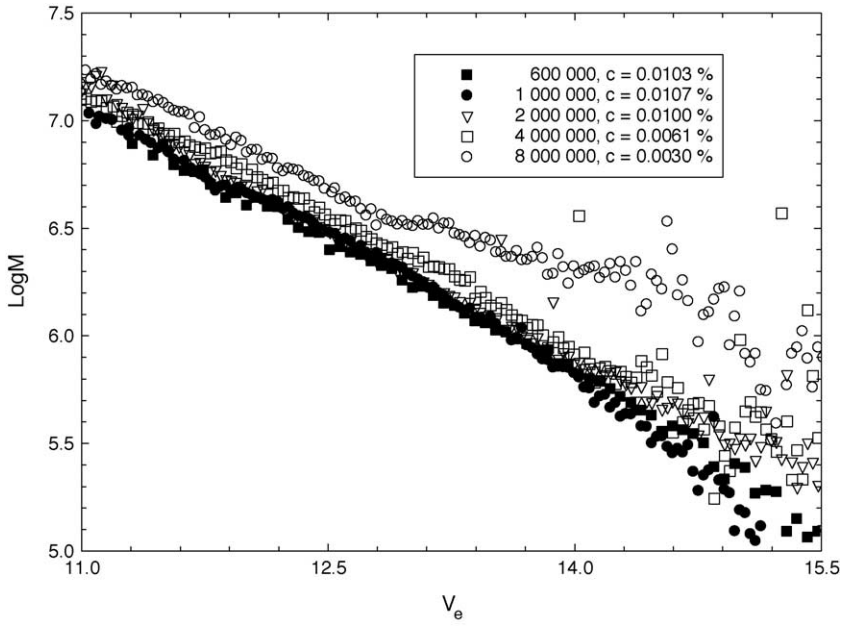

Fig. 10. Comparison of $\log M = f(V_e)$ calibrations of all investigated PEO samples obtained at 6 ml/h and optimized injected polymer concentrations.

The respective molecular masses and polydispersities of all samples investigated are presented in Table 3. The effect of the second virial coefficient term is shown to be low enough in all cases at injection concentrations used in the table. The molecular mass distributions of all samples obtained under optimized conditions are compared in Fig. 11 showing an increased asymmetry when M_w goes up.

SEC experiments with single RI detection were simulated at 6 ml/h using the average straight line fit of calibrations obtained for 600 000, 1 000 000 and 2 000 000 samples to calculate M_w and M_w/M_n of all samples using the respective RI

Table 3
PEO molecular masses and polydispersities obtained at 6 ml/h and optimized concentrations (SEC–LALS–RI)

Nominal M	c_{inj} (%)	$M_w \times 10^{-6}$	M_w/M_n	A_2 effect (%)
600 000	0.0103	0.859	3.8	1.6
1 000 000	0.0107	1.29	4.5	2.5
2 000 000	0.0100	2.09	4.1	2.9
4 000 000	0.0061	3.95	4.9	3.8
8 000 000	0.0030	6.95	4.2	3.5

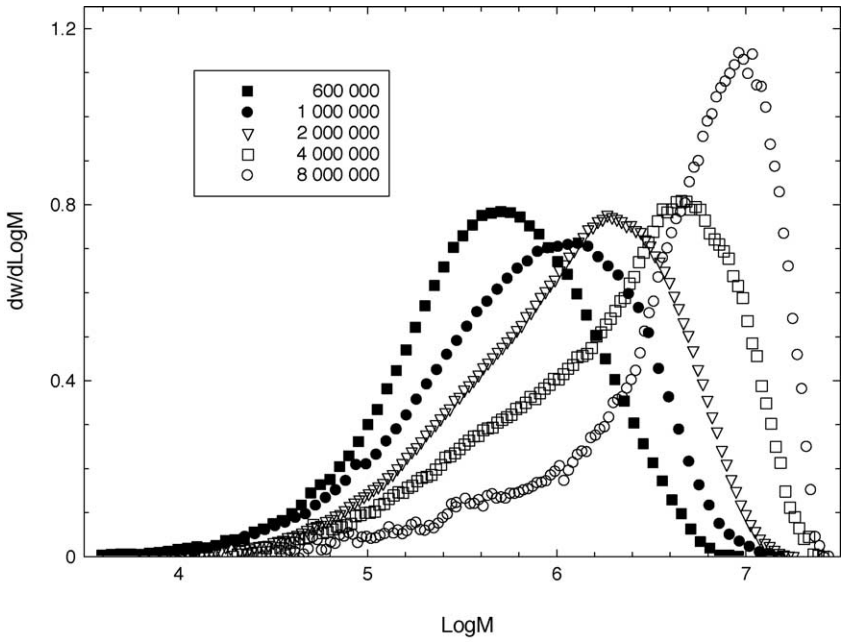

Fig. 11. Comparison of molecular mass distributions of all investigated PEO samples obtained at 6 ml/h and optimized injected polymer concentrations.

Table 4
Molecular masses and polydispersities of PEO samples investigated obtained from SEC–MALS–RI experiments at 0.1 ml/min and their deviations from SEC–LALS–RI data in Table 3

Nominal M	c_{inj} (%)	Berry 1st degree				Random coil			
		$M_w \times 10^{-6}$	ΔM_w (%)	M_w/M_n	$\Delta(M_w/M_n)$ (%)	$M_w \times 10^{-6}$	ΔM_w (%)	M_w/M_n	$\Delta(M_w/M_n)$ (%)
600 000	0.01	0.869[a]	+1.1	3.3	−13	0.930[a]	+8.2	4.3	+13
1 000 000	0.01	1.20[a]	−7.0	2.9	−36	1.31[a]	+1.5	3.6	−20
2 000 000	0.01	1.87[a]	−10.7	1.9	−54	2.13[a]	+1.9	2.3	−44
4 000 000	0.01	3.78[b]	−4.4	3.1	−37	3.85[b]	−2.5	5.0	+2
8 000 000	0.006	4.82[b]	−31	1.8	−57	4.93[b]	−30	2.8	−33

MALS detectors: superscripts (a) 4–18 and (b) 4–9.

peaks. As expected, very good agreement (within 5%) was obtained for the first three samples. The last two samples gave $M_w = 3.28 \times 10^6$ (−17.1%) and $M_w/M_n = 7.4$ and 4.66×10^6 (−33%) and 7.5, respectively. Hence, the dual detection, being more tolerant to the side effects discussed above, should be always preferred in SEC of UHM polymers.

The same set of PEO samples was investigated using MALS/RI detection. Similar distortions and/or shifts of $\log M = f(V_e)$ calibrations as shown above in the case of LALS detection were observed when injection concentration and/or flow-rate was varied. A typical example of distorted calibration obtained for PEO 4 000 000 at 0.2 ml/min and $c_{inj} = 0.025\%$ can be found in ref. [23]. Hence, the optimized injection concentrations found in LALS experiments were used at flow-rate 0.1 ml/min also here. The results in terms of M_w and M_w/M_n are summarized and compared with LALS results (Table 3) in Table 4. An additional difficulty was found in a lower RI sensitivity of the MALS/RI setup used. The injected concentration of the highest molecular mass samples, PEO 4 000 000 and 8 000 000, had to be somewhat increased to obtain reasonable signal-to-noise values of RI traces. It follows from the table that the increased injection concentration is acceptable only in the case of PEO 4 000 000 where a good agreement with LALS experiment was obtained. The MALS result for PEO 8 000 000 is obviously in error when compared with LALS values due to RI sensitivity/baseline problems. Hence, only remaining samples should be compared. Two angular extrapolation procedures were used as recommended in ref. [23]: the most robust Berry 1st degree plot and a forced random coil fit, certainly applicable to PEO. A good agreement between MALS and LALS M_w values is found in Table 4 independent of the choice of an extrapolation procedure. The random coil fit seems preferable improving somewhat the agreement of both M_w and M_w/M_n values. Nevertheless, the M_w/M_n values remain underestimated in two cases, also in the case of the random coil fit.

Molecular mass distributions obtained from MALS data are compared with LALS results in Fig. 12. A satisfactory agreement is found concerning the shape of the distributions, including their low-molecular mass side, despite of some underestimated values of M_n in Table 4. The extreme sensitivity of M_n to the presence of low-molecular mass component dis-

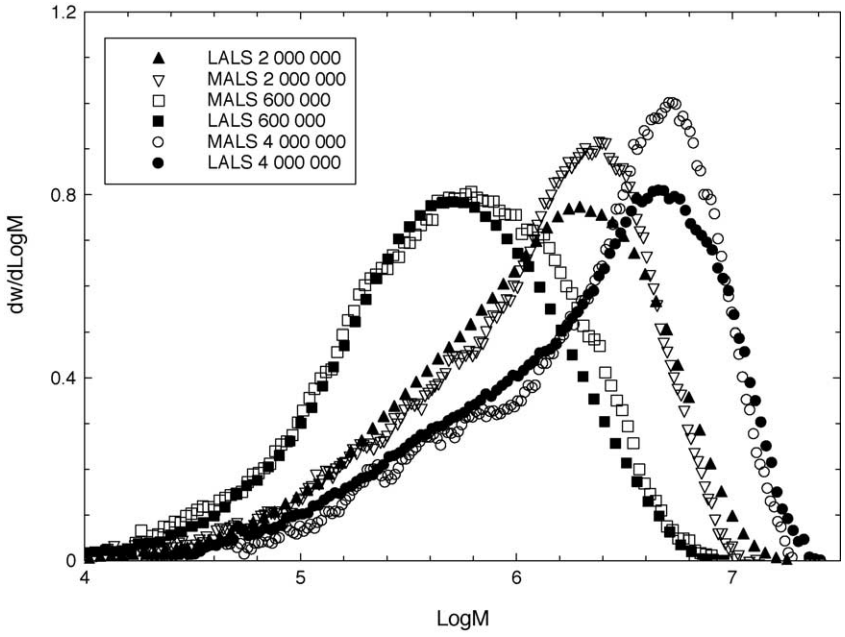

Fig. 12. Comparison of molecular mass distributions of PEO 600 000, 2 000 000 and 4 000 000 obtained from LALS/RI and MALS/RI experiments.

cussed above should be mentioned here as an explanation. Somewhat higher MALS distributions of PEO 2 000 000 and 4 000 000 are difficult to explain. Intuitively, it seems that this difference might result from the baseline error of RI signal rather than from the extrapolation error of LS signal. Thus, a reasonable agreement between LALS/RI and MALS/RI results (Table 4 and Fig. 12) can be obtained here provided that an optimized dissolution procedure, flow-rate, sample injection concentration and LS extrapolation procedure (in the case of MALS) are used.

Acknowledgment

B.P. wishes to thank the AstraZeneca R&D Mölndal and the Academy of Sciences of the Czech Republic (project no. AVOZ 4050913) for financial support. Miss Anna Asplund is acknowledged for experimental assistance.

References

[1] N. Clinton, P. Matlock, in: H.F. Mark, N.M. Bikales, Ch.G. Overberger, G. Menges, J.I. Kroschwitz (Eds.), Encyclopedia of Polymer Science and Engineering, vol. 6, second ed., John Wiley, New York, 1986, p. 225.
[2] J.C. Giddings, Adv. Chromatogr. 20 (1982) 217.
[3] K. Devanand, J.C. Selser, Macromolecules 24 (1994) 24.
[4] C.M. Kok, A. Rudin, Makromol. Chem. Rapid Commun. 2 (1981) 655.
[5] H.G. Barth, F.J. Carlin Jr., J. Liq. Chromatogr. 7 (1984) 1717.
[6] Y. Mei-Ling, S. Liang-He, J. Liq. Chromatogr. 5 (1982) 1259.
[7] P.J. Wang, B.S. Glasbrenner, J. Liq. Chromatogr. 10 (1987) 3047.
[8] E.V. Chubarova, V.V. Nesterov, J. Liq. Chromatogr. 13 (1990) 1825.
[9] M. Nakamura, Y. Ofusa, S. Mori, J. Liq. Chromatogr. Relat. Tech. 19 (1996) 339.
[10] M. Žigon, N.K. The, Ch. Shuyao, Z. Grubišič-Gallot, J. Liq. Chromatogr. Relat. Tech. 20 (1997) 2155.
[11] N. Aust, M. Parth, K. Lederer, Int. J. Polym. Anal. Charact. 6 (2001) 245.
[12] A.V. deGroot, W.J. Hamre, J. Chromatogr. 648 (1993) 33.
[13] A.R. D'Almeida, M.L. Dias, Polym. Degrad. Stab. 56 (1997) 331.
[14] W. Cheng, D. Hollis, J. Chromatogr. 408 (1987) 9.
[15] G. Stegeman, J.C. Kraak, H. Poppe, R. Tijssen, J. Chromatogr. A 657 (1993) 283.
[16] E. Venema, J.C. Kraak, H. Poppe, R. Tijssen, J. Chromatogr. A 740 (1996) 159.
[17] G. Stegeman, J.C. Kraak, H. Poppe, J. Chromatogr. 550 (1991) 721.
[18] Y.-C. Guillaume, J.-F. Robert, Ch. Guinchard, Anal. Chem. 73 (2001) 3059.
[19] A. Rudin, R.A. Wagner, J. Appl. Polym. Sci. 20 (1976) 1483.
[20] M.S. Song, G.X. Hu, X.Y. Li, B. Zhao, J. Chromatogr. A 961 (2002) 155.
[21] W. Brostow, M. Drewniak, N.N. Medvedev, Macromol. Theory Simul. 4 (1995) 745.
[22] E. Orviský, L. Šoltés, S. Al Assaf, Chromatographia 39 (1994) 366.
[23] M. Andersson, B. Wittgren, K.-G. Wahlund, Anal. Chem. 75 (2003) 4279.
[24] Union Carbide Corporation Safety data sheets of POLYOX® resins.
[25] W. Kaye, J. Colloid Interface Sci. 44 (1973) 384.
[26] R.K. Iler, The Chemistry of Silica, Wiley, New York, 1979.
[27] CAB-0-SIL® Fumed Silica, Cabot Corp. Available at: http://www.cabot-corp.com.